

The influence of radiation on ice crystal spectrum in the upper troposphere

Xiping Zeng*

Goddard Earth Sciences and Technology Center, University of Maryland, Baltimore County, and Laboratory for Atmospheres, NASA Goddard Space Flight Center, Greenbelt, Maryland, USA

ABSTRACT: This theoretical study is carried out to investigate the effect of radiation on ice crystal spectrum in the upper troposphere. First, an *explicit* expression is obtained for the ice crystal growth rate that takes account of radiative and kinetic effects. Second, the expression is used to quantitatively analyse how radiation broadens the ice crystal spectrum and then to reveal a new precipitation mechanism in the upper troposphere and the stratosphere. Third, the radiative effect is used to explain the subvisual clouds near the tropopause. Copyright © 2008 Royal Meteorological Society

KEY WORDS cirrus; subvisual cloud; precipitation

Received 18 March 2007; Revised 19 January 2008; Accepted 23 January 2008

1. Introduction

Tropical precipitation is still a challenge in meteorology (Simpson *et al.*, 1988). It involves multi-scale processes. Small-scale precipitating convection has a propensity to spontaneously organize into coherent structures or cloud clusters (e.g. Ludlam, 1980; Moncrieff, 2004), and cloud clusters in turn generate cloud shields in their mature and later stages (Zipser, 1969; Houze, 1977, 1982). Since cloud shields are widespread (or 10^4 – 10^5 km² in area; Houze, 1982; Nesbitt *et al.*, 2000), they modulate atmospheric radiation and thus change large-scale vertical circulations (Houze, 1982). As a feedback, large-scale circulations modify clouds and precipitation (Raymond and Zeng, 2005). In this multi-scale feedback, convective clouds and large-scale circulations are highly coupled through upper-tropospheric cirrus (e.g. Raymond and Zeng, 2000).

Theoretically speaking, cloud-resolving models can be used to evaluate the cirrus in the coupling between convective clouds and large-scale circulations. However, recent evaluations of cloud-resolving model simulations showed that the models predicted excessive clouds especially in the upper troposphere (e.g. Petch and Gray, 2001; Zeng *et al.*, 2007). Moreover, Starr and Quante (2002) compared the results of cirrus models using bin and bulk representation of microphysical processes. They pointed out that the bulk-parametrization model diagnosed a significant population of large ice particles while the bin model was dominated by small ice particles. Those modelling studies suggest that some physical processes are overlooked in the current cloud models.

Recent aircraft observations of ice particles (e.g. Heymsfield, 1986; Heymsfield *et al.*, 2006) have provided clues as to the processes that were overlooked in the current cloud models. Heymsfield (1986) showed that long-lasting subvisual clouds near the tropical tropopause consisted of ice crystals with small size and low number density. Heymsfield *et al.* (2006) reported that the maximum measured ice particle diameter increased with air temperature from -70 to -85 °C when convection existed below but decreased in the absence of deep convection.

Those modelling and observational issues may involve cloud–radiation interaction (see section 6 for discussion). Previous studies have proposed that radiation affects the diffusional growth of ice crystals (Hall and Pruppacher, 1976; Stephens, 1983; Hallett, 1987; Hallett *et al.*, 2002). Stephens (1983) showed that radiation significantly increases the survival distance of falling ice crystals in an unsaturated environment. He further suggested that the radiative effect on ice crystal growth be introduced in cloud models. However, few current cloud models (Wu *et al.*, 2000) account for it. One possible reason is that the ice crystal growth rate with the effect is expressed *implicitly* through the ice crystal surface temperature, making it less easy for a cloud model to adopt. Hence, it is imperative to obtain an explicit expression for the ice crystal growth rate first.

Accordingly, the radiative effect is studied in the present paper beginning with an explicit expression for the ice crystal growth rate. The expression is then used to quantitatively analyse how radiation broadens the ice crystal spectrum and finally to propose a new precipitation mechanism in the upper troposphere. The paper consists of seven sections. Section 2 describes a theoretical framework for ice crystal growth that takes

* Correspondence to: Xiping Zeng, Mail Code 613.1, NASA/Goddard Space Flight Center, Greenbelt, MD 20771, USA.
E-mail: zeng@agnes.gsfc.nasa.gov

account of radiative and kinetic effects. Sections 3 and 4 introduce linear and nonlinear models to show how radiation affects ice crystal spectrum, respectively. Section 5 presents a condition for haze aloft. Section 6 uses the present results to explain some clouds in the upper troposphere. Section 7 concludes. Except when specified, the paper follows the symbol definition in appendix A.

2. Theoretical framework

2.1. Heat balance of an ice crystal

The heat balance of an ice crystal in a rarefied atmosphere is represented by the following form (Hall and Pruppacher, 1976; Roach, 1976; Stephens, 1983; Hallett, 1987; Hallett *et al.*, 2002):

$$L_s 4\pi C D F_\beta \{\rho_{si}(T_s) - \rho_v\} f_m = 4\pi C K F_\alpha (T_e - T_s) f_Q + S F_s - S \varepsilon_0 \sigma (T_s^4 - \varepsilon_r \eta T_e^4), \quad (1)$$

where T_s and T_e refer to the ice crystal surface and the environmental air temperature, respectively; ρ_v and ρ_{si} denote the density of the ambient water vapour and saturated water vapour near a crystal, respectively; S denotes crystal surface area; f_m and f_Q are the ventilation factors expressed in Hall and Pruppacher (1976). Other factors are:

- (1) C – the stationary diffusion shape factor that accounts for the influence of crystal shape on the water vapour field around a crystal. For a spherical crystal of radius r , $C = r$.
- (2) D – the diffusivity of water vapour in air that is described by Hall and Pruppacher (1976):

$$D = 2.11 \times 10^{-5} (T/T_0)^{1.94} (p_0/p) \quad [\text{m}^2 \text{ s}^{-1}]. \quad (2)$$

- (3) K – the coefficient of thermal conductivity of dry air that is calculated with the formula of Beard and Pruppacher (1971)

$$K = \{2.38 + 0.00703(T - T_0)\} \times 10^{-2} [\text{J m}^{-1} \text{ s}^{-1} \text{ K}^{-1}],$$

which is independent of air pressure even when air pressure is low (N. Fukuta, 2004, personal communication).

- (4) F_β – a factor that accounts for the kinetic effect on water vapour diffusion. It is expressed as (Hall and Pruppacher, 1976)

$$F_\beta = r^*/(r^* + l_m^*) \quad (3)$$

where

$$r^* = S/4\pi C \quad (4)$$

$$l_m^* = \left(\frac{2\pi}{R_v T_s} \right)^{1/2} \frac{D f_m}{2\beta(2 - \beta)^{-1}}. \quad (5)$$

- (5) F_α – a factor that accounts for kinetic effect on heat diffusion. It takes the form (Fukuta and Walter, 1970; Carstens, 1972; Carstens *et al.*, 1974; Hall and Pruppacher, 1976; Pruppacher and Klett, 1997)

$$F_\alpha = r^*/(r^* + l_Q^*), \quad (6)$$

where

$$l_Q^* = \left(\frac{2\pi}{R_d T_s} \right)^{1/2} \frac{K f_Q}{\rho_a C_p 2\alpha(2 - \alpha)^{-1}}. \quad (7)$$

The factors $2\beta(2 - \beta)^{-1}$ and $2\alpha(2 - \alpha)^{-1}$ in (5) and (7) are referred to as the apparent deposition and thermal accommodation coefficients, respectively, (Chapman and Cowling, 1970; Fukuta, 2004 (In a copy of his manuscript ‘Advanced Cloud Physics’ received in 2004, N. Fukuta used the representative deposition coefficient and thermal accommodation coefficient to name the two factors, respectively.)) Based on experimental measurements (e.g. Fukuta and Walter, 1970; Shaw and Lamb, 1999), the thermal accommodation coefficient $\alpha = 0.7$, and the deposition coefficient $\beta = 0.04 \exp\{-(T - T_0)/85\}$ that fits the data of Fukuta and Walter (1970) when $T > -85^\circ\text{C}$.

- (6) F_s – the solar flux absorbed by an ice crystal.
- (7) ε_0 – the bulk absorption efficiency of an ice crystal for blackbody radiation. It is defined as the ratio of the infrared flux absorbed by a crystal to the radiative flux emitted by a blackbody at the crystal surface temperature. Based on the results of Stephens (1983), the efficiency is approximated with $\varepsilon_0 = 0.9\{1 - \exp(-r^*/6)\}$ for a crystal surface temperature of $T_{\text{ref}} = 261 \text{ K}$, where r^* is measured in micrometres. The Wien displacement law shows that the wavelength of peak emission for a blackbody is proportional to the reciprocal of temperature. Since radiation absorption depends on the dimensionless size parameter $2\pi r^*/\lambda$ where λ is radiation wavelength, the bulk absorption efficiency at temperature T is approximated with

$$\varepsilon_0(r^*, T) = 0.9\{1 - \exp(-Tr^*/6T_{\text{ref}})\}. \quad (8)$$

- (8) ε_r – the relative bulk absorption efficiency of an ice crystal for infrared radiation. It is defined as $\varepsilon/\varepsilon_0$ where ε represents the ratio of the infrared flux absorbed by a crystal to the infrared flux incident on the crystal. Let T_{min} and T_{max} denote the minimum and maximum temperature in the atmosphere and its underlying surface. The radiation emitted by a blackbody at temperature T_{min} and T_{max} may impinge on a crystal as two extreme limits. Hence,

$$\frac{\varepsilon_0(r^*, T_{\text{min}})}{\varepsilon_0(r^*, T)} < \varepsilon_r(r^*, T) < \frac{\varepsilon_0(r^*, T_{\text{max}})}{\varepsilon_0(r^*, T)},$$

which becomes

$$T_{\text{min}}/T < \varepsilon_r < T_{\text{max}}/T$$

with the aid of (8). Obviously, ϵ_r varies around unity. For the sake of simplicity, $\epsilon_r = 1$ is assumed except in section 5.

(9) η – the ratio of the infrared flux incident on crystal surface to the radiative flux emitted by a blackbody at the environmental air temperature. It is approximated with

$$\eta = \frac{F^+ + F^-}{2\sigma T_e^4}, \tag{9}$$

where F^+ and F^- represent the upward and downward fluxes of infrared radiation, respectively. Given a vertical distribution of atmospheric variables, the fluxes and thus η are determined by radiative processes (e.g. Fu and Liou, 1992; Chou *et al.*, 1995).

2.2. An explicit expression for ice crystal growth rate

The growth rate of an ice crystal is expressed in terms of ice crystal surface temperature T_s (e.g. Hall and Pruppacher, 1976). That is,

$$\frac{dm}{dt} = 4\pi C D F_\beta \{\rho_v - \rho_{si}(T_s)\} f_m, \tag{10}$$

where m is crystal mass. Next, (1) is used to eliminate T_s in (10) to derive an explicit expression for dm/dt .

To simplify the explicit expression and its derivation, a critical case of an ice crystal in a specific environment is considered first. In the environment, air temperature is still T_e , but humidity is so specific that the crystal does not grow or shrink. Let the symbol T_{sc} denote the crystal surface temperature, and e_c and H_{ic} denote the partial water vapour pressure and relative humidity in the critical case respectively, (The critical relative humidity H_{ic} is different from the effective radiative relative humidity defined by Hall and Pruppacher (1976). The latter is associated not only with the radiative effect on ice crystal growth but also the diffusivity of water vapour in air.). Thus, the crystal in the critical case has a heat balance between radiative cooling and conductive heating. That is,

$$S\epsilon_0\sigma(T_{sc}^4 - \epsilon_r\eta T_e^4) - SF_s = 4\pi C K F_\alpha(T_e - T_{sc})f_Q. \tag{11}$$

Since water vapour is spatially uniform in the critical case,

$$\rho_{si}(T_{sc}) = e_c(R_v T_e)^{-1}. \tag{12}$$

After introducing the symbol

$$\gamma \equiv (T_e - T_{sc})/T_e \tag{13}$$

and the approximation

$$T_{sc}^4 \approx T_e^4 + 4T_e^3(T_{sc} - T_e), \tag{14}$$

(11) is solved with

$$\gamma = \frac{\chi}{4(1 + \chi)} \left(1 - \epsilon_r\eta - \frac{F_s}{\epsilon_0\sigma T_e^4} \right) \tag{15}$$

where the symbol χ , as introduced in (20), represents the ratio of the infrared flux to the conductive heat flux from air to an ice crystal, where both air and ice crystal are treated as blackbodies.

$$\chi = \frac{S\epsilon_0\sigma T_e^3}{\pi C K F_\alpha f_Q}. \tag{16}$$

Using (12) and the ideal gas law for water vapour, the critical relative humidity $H_{ic} = e_c/E_{si}(T_e)$ is rewritten as

$$H_{ic} = \frac{T_e E_{si}(T_{sc})}{T_{sc} E_{si}(T_e)}. \tag{17}$$

This expression is changed further to

$$H_{ic} = \frac{1}{1 - \gamma} \left(1 - \frac{L_s\gamma}{R_v T_e} \right) \tag{18}$$

with the aid of (13), (15) and the approximation

$$\frac{E_{si}(T)}{E_{si}(T_e)} \approx \frac{L_s}{R_v} \frac{T - T_e}{T_e^2} + 1 \tag{19}$$

that is obtained from the Clausius–Clapeyron equation for when T is close to T_e .

Starting with expression (18) for the critical case, an explicit expression is derived next for the growth rate of an ice crystal in a general environment. Subtracting (11) from (1) yields

$$L_s 4\pi C D F_\beta \left\{ \rho_{si}(T_s) - \frac{(e T_{sc}/T_e)}{R_v T_{sc}} \right\} f_m = 4\pi C K (1 + \chi) F_\alpha (T_{sc} - T_e) f_Q, \tag{20}$$

using (14), (16) and the ideal gas law for water vapour. Equation (20) is still equivalent to (1) because the known variable T_{sc} always satisfies (11).

Fortunately, (20) is formally equivalent to the energy equation of the same crystal in an environment that is characterized as having an air temperature T_{sc} , partial water vapour pressure ($e T_{sc}/T_e$), coefficient of thermal conductivity $K(1 + \chi)$, and no radiative effect. Deriving the explicit expression for ice crystal growth rate, or the left side of (20), just as done in many textbooks on cloud physics (e.g. Rogers and Yau, 1989) gives

$$\frac{dm}{dt} = \frac{4\pi C}{A(T_{sc}) + B(T_{sc})} \left\{ \frac{(e T_{sc}/T_e)}{E_{si}(T_{sc})} - 1 \right\}, \tag{21}$$

where

$$A(T) = \frac{L_s}{F_\alpha f_Q K (1 + \chi) T} \left(\frac{L_s}{R_v T} - 1 \right) \tag{22}$$

$$B(T) = \frac{R_v T}{F_\beta f_m D E_{si}(T)}. \tag{23}$$

To remove T_{sc} from (21), $A(T_{sc})$ and $B(T_{sc})$ are changed to

$$A(T_{sc}) \approx A(T_e) \frac{T_e^2}{T_{sc}^2}$$

$$B(T_{sc}) \approx B(T_e) \frac{T_e E_{si}(T_e)}{T_{sc} E_{si}(T_{sc})}$$

with the aid of (2) and $|T_{sc} - T_e| \ll T_e$. Substituting (17) and the preceding two approximations into (21) yields an explicit expression for the growth rate of an ice crystal in a general environment. That is,

$$\frac{dm}{dt} = \frac{4\pi C(H_i - H_{ic})}{(1 - \gamma)^2 \{H_{ic} A(T_e) + B(T_e)\}}, \quad (24)$$

which does not involve T_s . Expression (24) shows that an ice crystal grows when relative humidity $H_i > H_{ic}$ and shrinks when $H_i < H_{ic}$. If $\varepsilon_r \eta = 1$ and $F_s = 0$, $H_{ic} = 100\%$, which reduces the expression into the traditional one without the radiative effect (e.g. Rogers and Yau, 1989).

Infrared and solar radiation affect H_{ic} . Due to $\gamma \ll 1$ and $\chi \ll 1$, (15) and (18) show that

$$(1 - H_{ic}) \propto \left(1 - \varepsilon_r \eta - \frac{F_s}{\varepsilon_0 \sigma T_e^4} \right).$$

Since infrared absorption of ice crystals is more important than solar absorption, the effect of solar radiation on ice crystal growth is neglected in the paper (i.e. $F_s/\varepsilon_0 \sigma T_e^4 = 0$). Next, H_{ic} is discussed by dividing $(1 - H_{ic})$ into two factors: $(1 - \varepsilon_r \eta)$ and $(1 - H_{ic})/(1 - \varepsilon_r \eta)$. The former factor involves radiative processes and the latter one depends on crystal size, shape and other non-radiative variables.

2.3. Infrared ratio η

The infrared ratio η approximately measures the relative magnitude of inward and outward infrared fluxes on the surface of an ice crystal. When $\varepsilon_r \eta < 1$, $H_{ic} < 100\%$ and thus radiation enhances crystal growth. Otherwise, $H_{ic} > 100\%$ and radiation benefits crystal shrinkage. Since η varies with the variables air temperature, water vapour and clouds, the following example is presented to show how η varies with height through the variables.

Consider the tropical atmosphere observed during the Kwajalein Experiment (KWAJEX) that was conducted around Kwajalein Atoll from 23 July to 15 September 1999. Figure 1 shows the mean air temperature and mixing ratio of water vapour versus pressure. Air temperature decreases considerably with pressure from 300 to 100 hPa.

Given a cloud distribution in the atmosphere, η is calculated using (9) and the code for radiative transfer (Chou *et al.*, 1995). Its results are displayed against pressure in Figure 2 for three given cloud distributions. When the sky is clear, $\eta > 1$ above the 250 hPa level and

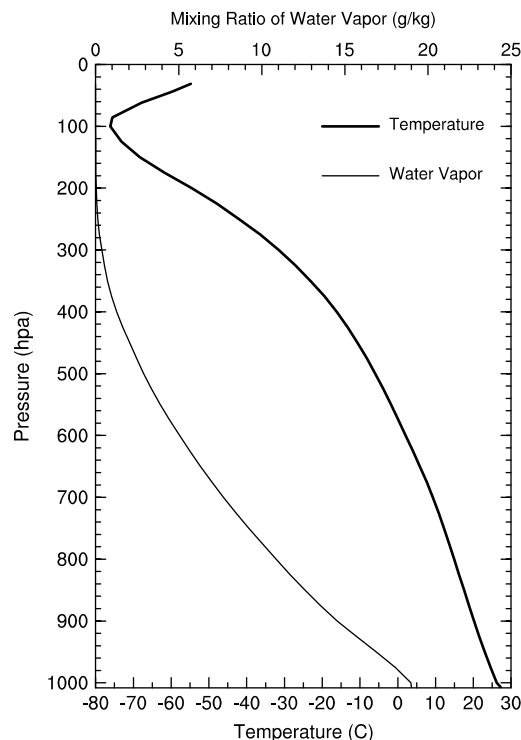


Figure 1. Vertical profiles of air temperature (thick line) and water vapour mixing ratio (thin line) obtained from averaging 52 days of KWAJEX data.

$\eta < 1$ below that height. The factor η reaches a minimum of 0.89 at 428 hPa and a maximum of 1.8 at 100 hPa. Comparing Figures 1 and 2 shows that the height for the maximum η corresponds to the height for the minimum temperature. Hence, η is largest at the tropopause.

Consider a thick stratiform cloud with the top at 600 hPa. Since the cloud behaves like a blackbody, η is close to unity in the cloud. Above the cloud, η varies with height similar to in a clear sky. Nevertheless, η is smaller than that for a clear sky, because the upward infrared flux decreases with decreasing the underlying blackbody temperature from the sea surface to cloud top.

Suppose the cloud top rises from 600 to 200 hPa. The cloud is so thick that it blocks the upward infrared radiation from the sea surface and the air below. Thus, it radiates upward as a blackbody but at a relatively low cloud-top temperature. Hence, high cirrus significantly decreases η and therefore greatly enhances the growth of ice crystals above itself.

2.4. The effect of crystal size and shape on H_{ic}

Once $\varepsilon_r \eta$ deviates from unity, the radiative effect on ice crystal growth is proportional to a ratio of $(1 - H_{ic})/(1 - \varepsilon_r \eta)$. The ratio depends on crystal size and shape as well as air temperature and pressure, which is discussed next.

Consider a spherical crystal. Given T and p , $(1 - H_{ic})/(1 - \varepsilon_r \eta)$ varies with radius. Figure 3 displays the ratio versus radius when $f_Q = 1$. The ratio increases with crystal size. Hence, H_{ic} decreases and increases with crystal size when $\eta < 1$ and $\eta > 1$, respectively, because

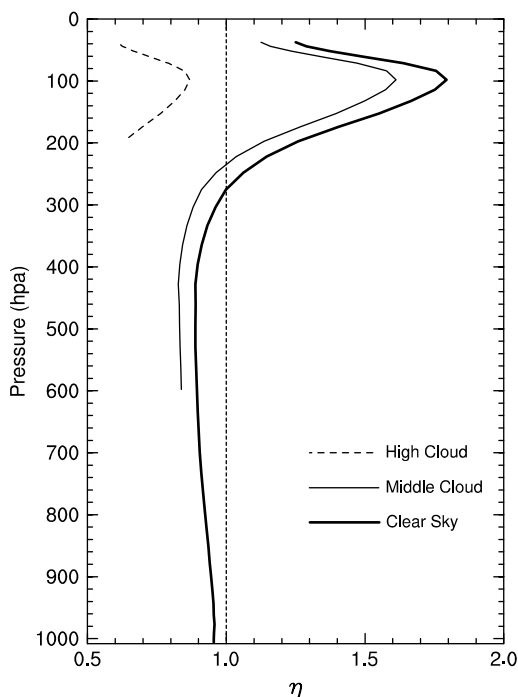


Figure 2. Infrared ratio η as a function of pressure. Thick, thin, and dashed lines represent cases with a clear sky, middle and high clouds, respectively.

ϵ_r is close to unity (see section 5 for the effect of ϵ_r on H_{ic}).

The ratio $(1 - H_{ic})/(1 - \epsilon_r \eta)$ also varies with height through air temperature and pressure. As shown in Figure 3, the ratio increases considerably with decreasing height. For example, it increases from 59 to 81% at $r^* = 1000 \mu\text{m}$ when (T, p) changes from $(-80^\circ\text{C}, 100 \text{ hPa})$ to $(-6^\circ\text{C}, 500 \text{ hPa})$.

Figure 3 is suitable for non-spherical crystals, too. A columnar-shaped crystal is modelled by a prolate spheroid of semi-major and minor axis lengths a and b , for which (Pruppacher and Klett, 1997)

$$C = \sqrt{a^2 - b^2} / \ln \left\{ \left(a + \sqrt{a^2 - b^2} \right) / b \right\}. \quad (25)$$

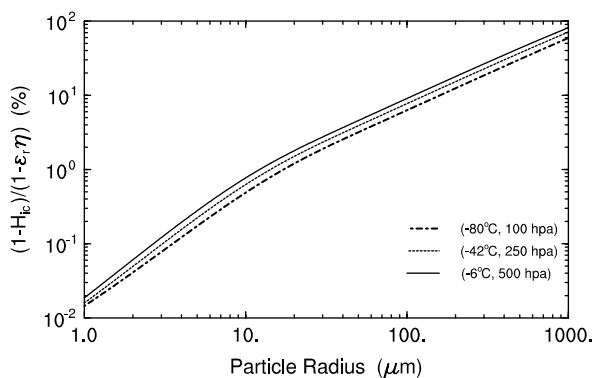


Figure 3. Critical relative humidity H_{ic} versus particle radius r^* , where thick dot-dashed, thin dashed, and solid lines represent the results when (T, p) equals $(-80^\circ\text{C}, 100 \text{ hPa})$, $(-42^\circ\text{C}, 250 \text{ hPa})$ and $(-6^\circ\text{C}, 500 \text{ hPa})$, respectively.

A plate-like ice crystal is modelled by an oblate spheroid of semi-major and minor axis lengths a and b , for which (Pruppacher and Klett, 1997)

$$C = \sqrt{a^2 - b^2} / \arcsin \sqrt{1 - b^2/a^2}. \quad (26)$$

After defining r^* in (4) and using it as the horizontal axis, Figure 3 displays as H_{ic} versus r^* for non-spherical crystals.

3. Two unsteady modes

3.1. A linear model

Expression (24) is used to analyse how radiation impacts ice crystal spectrum for a given relative humidity. Consider an ice crystal that deviates about its initial state; then (24) is linearized as

$$ds/dt = k(s_0)\{H_i - H_{ic}(s_0)\} + (s - s_0)/\tau(s_0), \quad (27)$$

where subscript '0' indicates the initial state and

$$s = 4\pi r^{*2} \quad (28)$$

$$\tau(s) = -\{k(s)dH_{ic}/ds\}^{-1} \quad (29)$$

$$k(s) = \frac{4\pi C}{(1 - \gamma)^2\{H_{ic}A(T_e) + B(T_e)\}} \left(\frac{dm}{ds} \right)^{-1}. \quad (30)$$

Buoyancy waves and underlying clouds modulate H_i and H_{ic} , respectively. Without loss of generality, suppose that

$$H_i - H_{ic}(s_0) = \Delta H_{i0} + A_H \sin(\omega t), \quad (31)$$

where the forcing parameters ΔH_{i0} , A_H and ω are constant. Substituting (31) into (27) and then solving the resulting equation yields

$$s - s_0 = -\frac{kA_H}{\tau^{-2} + \omega^2} [\tau^{-1} \sin(\omega t) + \omega \{\cos(\omega t) - 1\}] + k\Delta H_{i0}\tau(e^{t/\tau} - 1) + \frac{kA_H(\omega\tau)}{1 + (\omega\tau)^2} \tau(e^{t/\tau} - 1) \quad (32)$$

where k and τ take their values at $s = s_0$. As shown in the preceding equation, crystal growth accelerates when $A_H > 0$ and $\Delta H_{i0} > 0$, and shrinkage is enhanced when $A_H < 0$ and $\Delta H_{i0} < 0$. These two unsteady modes broaden and narrow the ice crystal spectrum when $\eta < 1$ and $\eta > 1$, respectively, which is detailed in subsection 4.2.

The third term on the right-hand side of (32) represents the bulk ice crystal growth in a period due to a buoyancy wave or underlying-cloud variation. It has a factor of $(\omega\tau)/\{1 + (\omega\tau)^2\}$, which reaches a maximum at $\omega\tau = 1$. For a given τ , the factor (or the spectrum broadening) is directly proportional to the forcing period $2\pi/\omega$ when $\omega\tau \gg 1$ and inversely proportional to the forcing period when $\omega\tau \ll 1$.

3.2. Time-scale for spectrum broadening

The second and third terms on the right-hand side of (32) share a common factor of $\tau(e^{t/\tau} - 1)$ that is inversely proportional to τ . For solid spherical crystals without involving radiation, $\tau \rightarrow \infty$, which results in $\tau(e^{t/\tau} - 1) = 0$. Hence, an ice crystal spectrum with $|\tau| < \infty$ is broadened or narrowed with respect to a spectrum with $\tau \rightarrow \infty$. In brief, τ measures the spectrum broadening (or narrowing) due to radiation.

The time-scale τ relies on ε_r , η , crystal size, shape, air temperature and pressure. As shown by (15), (18) and (29), τ is almost inversely proportional to $1 - \varepsilon_r \eta$. Thus, the next discussions address $\tau(1 - \varepsilon_r \eta)$ versus crystal size and shape first and then air temperature and pressure.

Figure 4 displays $\tau(1 - \varepsilon_r \eta)$ versus r^* for five crystal shapes when the air temperature and pressure equal -80°C and 100 hPa, respectively. Using ice crystal parameters from observations, the time-scale is calculated with (29), which is detailed next.

- A graupel particle is treated as a sphere with a bulk ice density of 0.9 g kg^{-1} and ventilation factors f_m and f_Q are assumed to be both unity. This crystal shape is so simple that τ versus r^* is easily understood with (28)–(30). Thus, the shape is discussed here as a reference for other shapes. Figure 4 displays the time-scale $\tau(1 - \varepsilon_r \eta)$ of graupel against r^* . The time-scale decreases and increases with r^* when r^* is small and large, respectively. It reaches a minimum of 3.5 days at $r^* = 5 \text{ }\mu\text{m}$.
- A bullet-shaped crystal is modelled with a prolate spheroid of semi-major and minor axis lengths a and b , for which the surface area is

$$S = 2\pi b \left(b + \frac{a^2}{\sqrt{a^2 - b^2}} \arcsin \frac{\sqrt{a^2 - b^2}}{a} \right). \quad (33)$$

The expressions for the mass and terminal velocity of bullets come from Heymsfield and Iaquinta (2000); the expression for the dimensional relationship from Heymsfield (1972); and the expressions for the ventilation factors from Hall and Pruppacher (1976). Using those

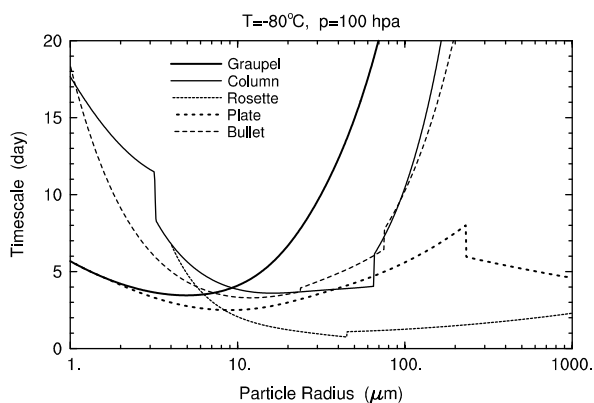


Figure 4. Time-scale $\tau(1 - \varepsilon_r \eta)$ versus particle radius r^* for five crystal shapes when (T, p) equals $(-80^\circ\text{C}, 100 \text{ hPa})$.

expressions, the time-scale for single bullets is calculated and shown against r^* in Figure 4. The curves of time-scale versus r^* are not smooth because the curves for crystal parameters (e.g. mass, dimensional relationship) versus size are not smooth either. Generally speaking, the time-scale curve for single bullets is similar to that for graupel except that $\tau(1 - \varepsilon_r \eta)$ reaches a minimum of 3.3 days at $r^* = 12 \text{ }\mu\text{m}$.

- A plate-like crystal is modelled with an oblate spheroid of semi-major and minor axis lengths a and b , for which

$$S = 2\pi a \left(a + \frac{b^2}{\sqrt{a^2 - b^2}} \ln \frac{\sqrt{a^2 - b^2} + a}{b} \right). \quad (34)$$

The mass of the plates with dendritic extensions is calculated with the bulk density of Heymsfield (1972). The dimensional relationship of the plates is determined with the observations of Auer and Veal (1970). The terminal velocity is calculated with the expression of Heymsfield (1972). With those relationships, the time-scale for plate-like crystals is calculated and shown against r^* in Figure 4. In contrast to graupel, plate-like crystals have a similar time-scale versus r^* except that $\tau(1 - \varepsilon_r \eta)$ reaches a minimum of 2.5 days at $r^* = 8.9 \text{ }\mu\text{m}$ when $r^* < 200 \text{ }\mu\text{m}$. The decrease in time-scale at $r^* = 200 \text{ }\mu\text{m}$ coincides with the emergence of dendritic extensions at that size.

- A column-like crystal is modelled with a prolate spheroid. The expressions for the mass and terminal velocity of columns come from Heymsfield and Iaquinta (2000), and that for the dimensional relationship from Auer and Veal (1970) and Heymsfield (1972). Figure 4 displays the time-scale for column-like crystals against r^* and shows that $\tau(1 - \varepsilon_r \eta)$ is close to 3.6 days when r^* is between 10 and 60 μm .
- A rosette crystal consists of bullets. It is modelled approximately with a sphere. In the present paper, rosettes with four bullets are assumed unless specified. The mass and terminal velocity of rosettes are calculated with the formulae of Heymsfield and Iaquinta (2000). Figure 4 also displays the time-scale for the rosettes against r^* and shows that $\tau(1 - \varepsilon_r \eta)$ reaches a minimum of 0.75 day at $r^* = 44.8 \text{ }\mu\text{m}$.

The time-scale for spectrum broadening, as summarized in Figure 4, varies with crystal shape. It varies with crystal size similarly for different shapes. Moreover, it varies considerably with height via air temperature and pressure. Figure 5 displays the time-scale versus r^* when (T, p) equals $(-42^\circ\text{C}, 250 \text{ hPa})$ and $(-6^\circ\text{C}, 500 \text{ hPa})$, respectively. In comparison to Figure 4, the figure shows that the time-scale versus r^* is similar at different heights, but the time-scale increases significantly with height. These characteristics of the time-scale are helpful in understanding the numerical results in the next section.

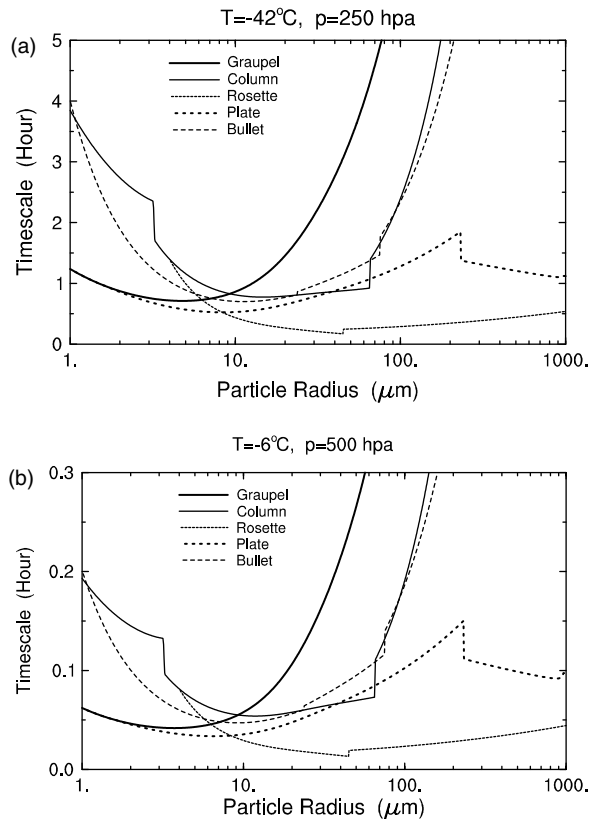


Figure 5. Same as in Figure 4 except that (T, p) equals $(-42^\circ\text{C}, 250 \text{ hPa})$ and $(-6^\circ\text{C}, 500 \text{ hPa})$ in the upper and lower panels, respectively.

4. Numerical simulations

The preceding linear model deals with the radiative effect while H_i is given. Since crystal growth consumes water vapour, H_i changes with time. Next, a nonlinear model that uses H_i as a prognostic variable is introduced to show the radiative effect in a general framework.

4.1. A nonlinear model

Consider an air parcel that moves vertically. Based on the conservation of energy and water, its relative humidity is governed by

$$\frac{dH_i}{dt} = Q_1(T_e)w - Q_2(T_e) \sum_j \frac{dm_j}{dt}, \tag{35}$$

where $m_j (j = 1, 2, \dots)$ denotes the mass of different sized ice crystals, and

$$Q_1(T) = \frac{1}{T} \left(\frac{L_s g}{R_v C_p T} - \frac{g}{R_d} \right) \tag{36}$$

$$Q_2(T) = \rho_a \left(\frac{R_v T}{E_{si}(T)} + \frac{R_d L_s^2}{p R_v C_p T} \right). \tag{37}$$

The expressions for Q_1 and Q_2 are derived similarly to that for water vapour condensation in Rogers and Yau (1989, p.106). Since the present crystal growth rate

takes account of the radiative effect, this parcel model represents the radiative effect on ice crystal spectrum.

To model the spectrum evolution accurately, (24) is changed to

$$\frac{da^2}{dt} = \frac{4\pi C(H_i - H_{ic})}{(1 - \gamma)^2 \{H_{ic} A(T) + B(T)\}} \left(\frac{dm}{da^2} \right)^{-1}, \tag{38}$$

which uses a^2 rather than a as a prognostic variable because the term on the right-hand side of (38) is almost constant for spherical crystals. In the following numerical simulations, (35) and (38) are used as prognostic equations and are integrated with 1024 bins.

4.2. A mechanism for precipitation formation

Consider a stationary air parcel with $\epsilon_r = 1$ and a constant η . Based on the linear model in the preceding section, the evolution of the ice crystal spectrum is reasoned as follows. Since $(1 - H_{ic})/(1 - \eta)$ increases with crystal size, H_i changes so that eventually it lies between H_{ic} for small and large crystals, no matter what the initial relative humidity is. When $\eta < 1$, H_i is lower than H_{ic} for small crystals but higher than that for large ones. As a result, small crystals shrink due to sublimation with some eventually disappearing. Large crystals grow due to deposition with some of them becoming precipitating crystals. This sublimation–deposition process broadens the ice crystal spectrum, and therefore converts cloud ice to precipitation. In contrast, when $\eta > 1$, H_i is higher than H_{ic} for small crystals but lower than that for large ones. As a result, large crystals shrink due to sublimation while small ones grow due to deposition, narrowing the ice crystal spectrum.

To support this reasoning, a default numerical experiment is done to simulate plate-like crystal growth in an air parcel near the tropopause. Suppose that $T = -80^\circ\text{C}$, $p = 100 \text{ hPa}$ and the initial spectrum of ice crystals is

$$dN(a) = c_1 a e^{-c_2 a} da, \tag{39}$$

where $N(a)$ denotes the number of ice crystals with the semi-major axis length less than a . After choosing $c_1 = 1.25 \times 10^{16} \text{ m}^{-5}$ and $c_2 = 0.5 \mu\text{m}^{-1}$, the initial concentration of ice crystals is $5 \times 10^4 \text{ m}^{-3}$ and the ice water content $9 \times 10^{-6} \text{ g m}^{-3}$, close to observations for subvisual clouds (Heymsfield 1986). Given $\eta = 0.5$ and the initial relative humidity $H_i = 100\%$, the ice crystal spectrum and H_i are simulated using the time step $\Delta t = 8 \text{ s}$. The modelled H_i is displayed against time in Figure 6. It decreases slowly with time. Meanwhile, the ice water content increases slowly due to water conservation (figure omitted).

Figure 7 shows the evolution of the mass density $dM(a)/d \ln(a)$ from $t = 0$ to 20 days, where $M(a)$ represents the mass of ice crystals with the semi-major axis length less than a . As shown in the figure, small crystals shrink due to sublimation and large ones grow due to deposition. Correspondingly, the median size of

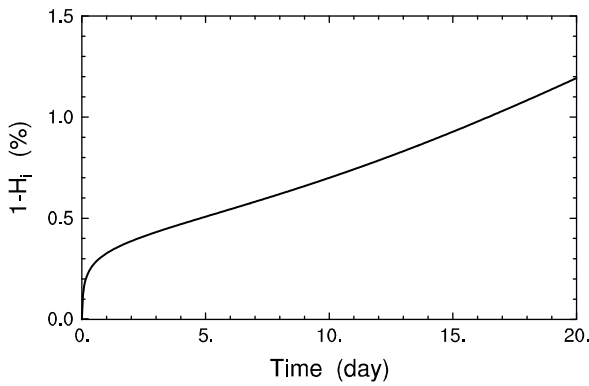


Figure 6. Relative humidity H_i versus time in the default experiment where $T = -80^\circ\text{C}$, $p = 100$ hPa and $\eta = 0.5$.

ice crystals increases with time. Since the small and large crystals grow oppositely, H_i lies between the H_{ic} for small and large crystals. Hence, H_i is close to the H_{ic} for the median size crystals. The increase in median crystal size corresponds to the decrease in H_i shown in Figure 6.

If no radiation is involved (or $\eta = 1$), the ice crystal spectrum and H_i remain at their initial state. Hence, radiation is responsible for the spectrum broadening shown in Figure 7.

To show the radiative effect when $\eta > 1$, the default experiment is redone after increasing η from 0.5 to 1.5 and using the final spectrum in Figure 7 as the initial one. Since (35) and (38) are symmetric with respect to $\eta = 1$, it is easily inferred that the spectrum evolution with $\eta = 1.5$ reverses that shown in Figure 7. Hence, large crystals shrink due to sublimation and small ones grow due to deposition when $\eta > 1$. In other words, radiation narrows the ice crystal spectrum when $\eta > 1$.

4.3. Sensitivity of precipitation formation to height

The preceding subsection reveals that precipitation can form on a time-scale of days at 100 hPa when $\eta < 1$. Here, two additional experiments with $\eta = 0.5$ are carried out to show that precipitation forms faster at lower heights for the same η . The first additional experiment

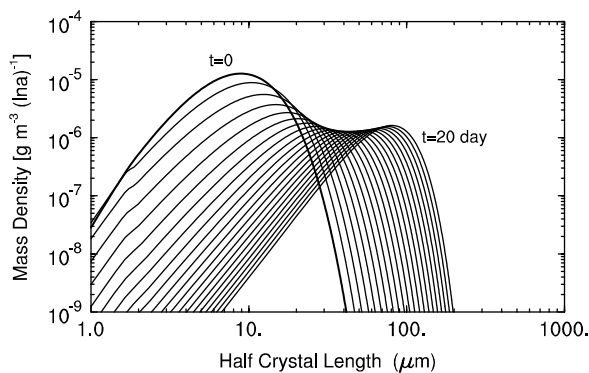


Figure 7. Evolution of the mass density $dM(a)/d \ln(a)$ versus the half crystal size a in the default experiment where $T = -80^\circ\text{C}$ and $p = 100$ hPa. The thick line denotes the initial spectrum, and the time interval between lines is 1 day.

uses the same parameters as the default one except for $T = -42^\circ\text{C}$ and $p = 250$ hPa. In the experiment, a parameter for initial ice crystal spectrum $c_1 = 1.25 \times 10^{18} \text{ m}^{-5}$, which corresponds to an initial crystal concentration of $5 \times 10^6 \text{ m}^{-3}$ and an ice water content of $9 \times 10^{-4} \text{ g m}^{-3}$. The experiment is performed with a time step $\Delta t = 0.5$ s. Figure 8 displays the evolution of the mass density from $t = 0$ to 6 hours, showing that precipitation can form on a time-scale of hours at 250 hPa, much shorter than that at 100 hPa.

The second additional experiment uses the same parameters as the first additional one except for $T = -6^\circ\text{C}$ and $p = 500$ hPa. The experiment was performed with $\Delta t = 0.02$ s. Figure 9 displays the evolution of the mass density from $t = 0$ to 15 minutes, revealing that precipitation can form on a time-scale of ten minutes at $p = 500$ hPa. In summary, precipitation formation due to radiation is sensitive to height via air temperature and pressure. This sensitivity of precipitation formation to height is a result of the sensitivity of the time-scale to height shown in Figures 4 and 5.

5. Spectral asymmetry between absorbed and emitted radiation

Consider an optically thin cloud in a clear stationary atmosphere. The cloud is so thin that it has almost

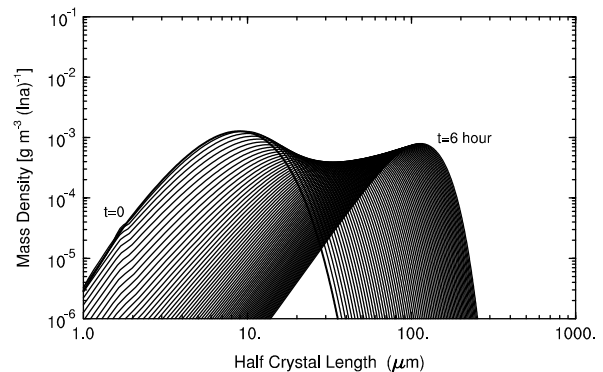


Figure 8. Same as in Figure 7 except that $T = -42^\circ\text{C}$, $p = 250$ hPa and the time interval between lines is 5 minutes.

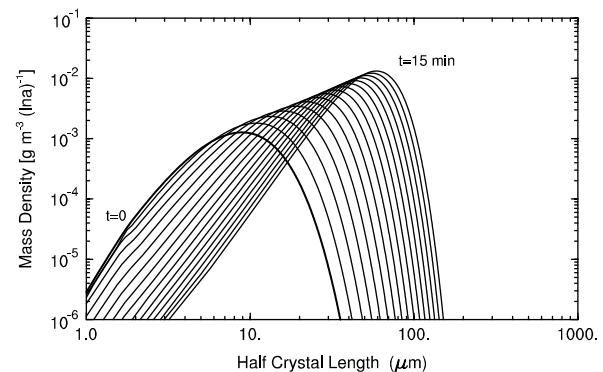


Figure 9. Same as in Figure 7 except that $T = -6^\circ\text{C}$, $p = 500$ hPa and the time interval between lines is 1 minute.

no effect on atmospheric radiation. Thus, much of the infrared radiation emitted by the underlying surface can reach the crystals in the cloud through the atmospheric thermal infrared window, leading to an obvious spectral asymmetry between crystal-absorbed and emitted radiation (or $\epsilon_r \neq 1$). Next, a crystal in the cloud is discussed as an example to show the effect of the spectral asymmetry on H_{ic} .

For an ice crystal in the cloud, ϵ_r is close to its maximum, or

$$\epsilon_r \approx \epsilon_0(r^*, T_{ust})/\epsilon_0(r^*, T) \tag{40}$$

where T_{ust} is the underlying surface temperature. Equations (8) and (40) show that $\epsilon_r > 1$ while $T < T_{ust}$.

The infrared ratio η , just as shown in Figure 2, is larger than unity in the upper troposphere but smaller than unity in the middle and lower troposphere. Consider an ice crystal with an environment of $\eta = 1.8$, $T = -80^\circ\text{C}$, $p = 100$ hPa, and $T_{ust} = 300$ K. Using ϵ_r in (40), H_{ic} is calculated and displayed against r^* in Figure 10. Meanwhile, the H_{ic} with $\epsilon_r = 1$ is displayed in the same figure for comparison. Obviously, ϵ_r affects H_{ic} considerably when $r^* < 40 \mu\text{m}$. It changes H_{ic} by 0.2% at $r^* = 12 \mu\text{m}$. Since ϵ_r does not reverse the increase in H_{ic} with increasing r^* , it affects the sublimation–deposition process only quantitatively while $\eta > 1$.

In contrast, consider a crystal with an environment of $\eta = 0.9$, $T = -12^\circ\text{C}$, $p = 430$ hPa and $T_{ust} = 300$ K. Using ϵ_r in (40), H_{ic} is calculated and displayed in Figure 11. It increases and decreases with r^* while r^* is smaller and larger than $r_{MAX}^* = 1.9 \mu\text{m}$, respectively. In other words, H_{ic} reaches a maximum of $H_{icMAX} = 1 + 6 \times 10^{-6}\%$ at $r^* = r_{MAX}^*$. When $1 < H_i < H_{icMAX}$, there are two equilibrium states (or $H_i = H_{ic}(r^*)$) for an ice crystal. The equilibrium state with the smaller r^* is stable, corresponding to haze aloft. The other equilibrium state with the larger r^* is unstable. A crystal at the unstable equilibrium state, once perturbed initially, either

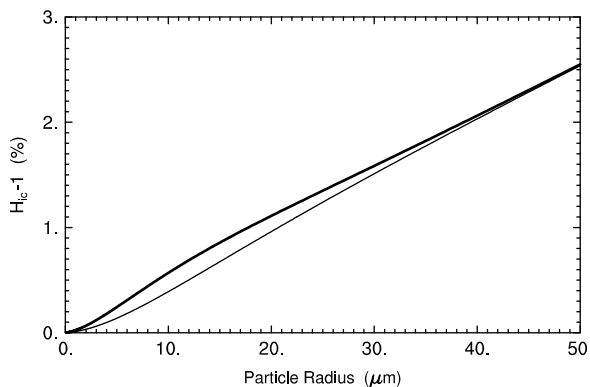


Figure 10. Critical relative humidity H_{ic} as a function of particle radius r^* , where $\eta = 1.8$, $T = -80^\circ\text{C}$, $p = 100$ hPa and $T_{ust} = 300$ K. The thin and thick lines represent H_{ic} when ϵ_r equals one and is calculated with (40), respectively.

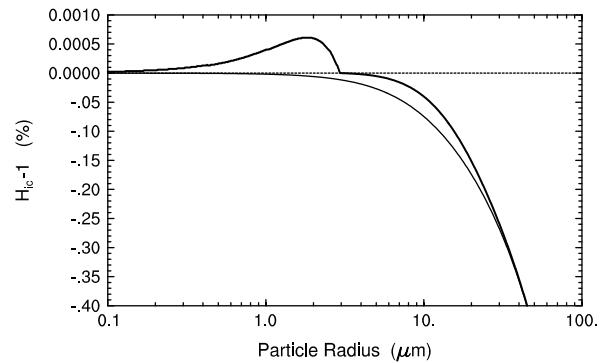


Figure 11. Critical relative humidity H_{ic} as a function of particle radius r^* , where $\eta = 0.9$, $T = -12^\circ\text{C}$, $p = 430$ hPa and $T_{ust} = 300$ K. The thin and thick lines represent H_{ic} when ϵ_r equals unity and is calculated with (40), respectively.

shrinks to reach the stable state or grows to become a precipitating crystal.

When many ice crystals coexist under $\eta < 1$ and some of them have H_{ic} less than 100%, the sublimation–deposition process works to form precipitation just as in the atmosphere with $\epsilon_r = 1$. In summary, ϵ_r cannot change the sublimation–deposition process greatly even while $\eta < 1$.

6. Discussion

The preceding sections proposed a precipitation mechanism: when $\eta < 1$, the sublimation–deposition process due to radiation converts cloud ice to precipitating ice that in turn sediments to dehumidify air. This process, different from particle sedimentation, can work as a source of large particles near cloud top. Next, cloud-top observations are discussed to infer the existence of the process.

6.1. Subvisual clouds

Heymsfield (1986) observed the microphysical structure of subvisual clouds near the tropical tropopause and showed that the clouds consist of ice particles with a mean diameter of $2.5 \mu\text{m}$ and number density of less than $5 \times 10^4 \text{ m}^{-3}$. The subvisual clouds are common, but not pervasive, in the Tropics and subtropics (Winker and Trepte, 1998). They are separated from cirrus below but tend to occur with thick cirrus below (Heymsfield, 1986; Winker and Trepte, 1998). They can also persist for weeks or months in clear skies in the equatorial regions (Lynch and Sassen, 2002). These observations match the characteristics of the radiative effect, which is shown next.

In the Tropics, convective clouds drive large-scale upward motion in the troposphere (Riehl and Malkus, 1958). Thus, horizontal water advection cannot generate subvisual clouds near the tropopause. On the other hand, local vertical circulations (including turbulent motions) transport water downgradient near the tropopause. As a result, water accumulates near the tropopause, and thus pervasive clouds are expected there.

The sublimation–deposition process due to radiation can break the pervasive clouds into subvisual clouds. Since high cirrus leads to $\eta < 1$ near the tropopause (see Figure 2), the process, accompanied by high cirrus below, can convert small ice crystals to large ones that in turn sediment, serving as a water sink near the tropopause. Owing to the maximum η and minimum T at the tropopause, the conversion of cloud ice to precipitation is the least efficient there. As a result, the process can separate subvisual clouds from cirrus below. With the aid of the sublimation–deposition process, high cirrus can enlarge the crystals near the tropopause that in turn radiate upwards strongly, which resembles the satellite-observed positive correlation between subvisual clouds and the thick cirrus below.

In the absence of high cirrus, $\eta > 1$ near the tropopause and large crystals shrink there, which can explain the small size of ice crystals in subvisual clouds. Since ice crystals shrink on a time-scale of 10 days (see Figures 4 and 7), subvisual clouds can last for weeks or months in clear skies. In summary, the observations of subvisual clouds match the characteristics of the radiative effect, which suggests that the sublimation–deposition process exists near the tropopause.

6.2. Vertical distributions of ice crystal spectrum

Heymsfield *et al.* (2006) observed large crystals with a scale up to $10^3 \mu\text{m}$ at -85°C . They reported that the maximum measured ice particle diameter increased from -70 to -85°C when convection existed below. That observational phenomenon, involving the origin of large crystals right below the tropopause, can be explained partly by the radiative effect.

Suppose that convective cells eject ice crystals into the upper troposphere (Heymsfield *et al.*, 2006), which are then blown by the horizontal wind to form a stratiform cloud. The cloud in turn imposes a perturbation on the original vertical η distribution. Consider, for example, a stratiform cloud in the atmosphere as discussed in Figure 1. When the cloud has a constant cloud ice mixing ratio of 0.1 g/kg from 132 to 197 hPa, it introduces an η perturbation as shown in Figure 12. Since $\eta < 1$ near cloud top, radiation can broaden the ice crystal spectrum there. In contrast, $\eta > 1$ near cloud base, which means that radiation narrows the spectrum there (Stephens, 1983). Thus, the radiative effect contributes to the increase in the maximum crystal size with height.

The stratiform cloud discussed in Figure 12 is optically thick. It imposes a strong perturbation on the original vertical η distribution so that $\eta < 1$ in a layer. However, an optically thin cloud introduces a weak η perturbation so that there is no layer with $\eta < 1$ and therefore no layer with spectrum broadening. If convective clouds and their anvils arise below a thin cloud, η above the convective clouds is decreased. As a result, $\eta < 1$ near the top of the thin cloud and $\eta > 1$ near the base, which contributes to an increase in the maximum ice crystal size with height and partly explains the observational phenomenon that

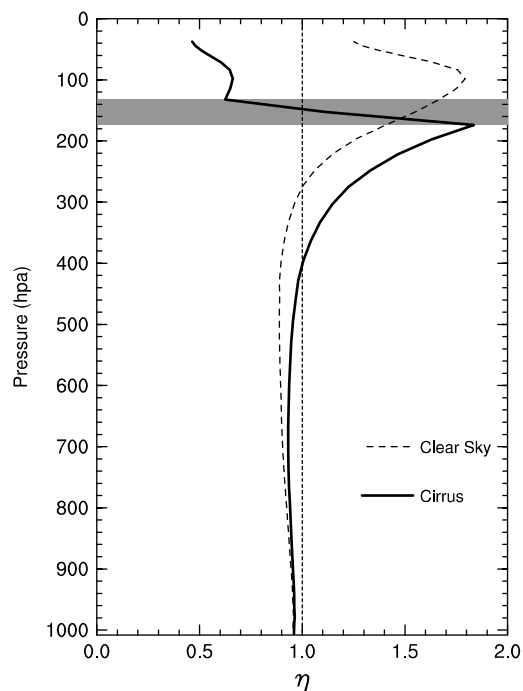


Figure 12. Infrared ratio η as a function of pressure for two cases. The thick line represents a case for a cloud (denoted by the shaded area). The dashed line represents a case for a clear sky.

the maximum measured ice particle diameter increased from -70 to -85°C when convection existed below.

6.3. Cumulus cloud seeding

Precipitation initiation in warm cumulus clouds involves the formation of large drops on the scale of cloud lifetimes (e.g. 15 minutes). It requires some process to accelerate the growth of drops at a radius of $\sim 20 \mu\text{m}$ where neither diffusional nor collectional growth is significant. Current theories (e.g. giant salt particles, drop collision due to turbulence, and cloud entrainment) still involve some uncertainties (e.g. Rogers and Yau, 1989; Pruppacher and Klett, 1997), such that the precipitation initiation is not yet fully understood. Based on the present study, the radiative effect is proposed as a candidate to initiate precipitation in warm cumulus clouds.

Consider a number of crystals in a blue sky. They form due to gravity waves (or other processes) and some of them have length greater than $\sim 4 \mu\text{m}$. Since $\eta < 1$ below the height of the 250 hPa level (see Figure 2), a part of the crystals can grow to become precipitating ones (see section 5) that fall and then melt below the freezing level. Once the precipitating particles fall into cumulus clouds, they can serve as seeds to initiate frequent collision between drops, which would in turn generate precipitation quickly. From another perspective, radiation can broaden the cloud spectrum near cloud top. Following the same procedure with (24) except for variables for liquid water, an explicit expression for the critical relative humidity with respect to water H_{wc} is obtained. Since H_{wc} functions in a similar manner as H_{ic} and $\eta < 1$ near cloud top, radiation can broaden the cloud

spectrum there and thus contribute partly to precipitation initiation.

In the preceding three cases, the radiative effect is expected to provide large particles near cloud top. Based on the consistence between the characteristics of the radiative effect and the observations of subvisual clouds, it is inferred that the sublimation–deposition process exists in the upper troposphere. Using the present explicit expression for ice crystal growth rate, the radiative effect will be incorporated into a cloud-resolving model for further evaluation.

7. Conclusions

This theoretical study addresses the effect of radiation on ice crystal spectrum. From the heat balance equation of an ice crystal, an explicit expression for ice crystal growth rate is obtained that takes account of the radiative effect. The expression introduces three variables: the critical relative humidity H_{ic} , the infrared ratio η , and the relative bulk absorption efficiency ε_r . An ice crystal grows and shrinks when the relative humidity $H_i > H_{ic}$ and $H_i < H_{ic}$, respectively.

The critical relative humidity H_{ic} is associated with η through an approximately linear relationship between $(1 - H_{ic})$ and $(1 - \varepsilon_r \eta)$ when the effect of solar radiation is ignored. The ratio $(1 - H_{ic})/(1 - \varepsilon_r \eta)$ depends on crystal size and shape as well as air temperature and pressure. Generally speaking, the ratio increases with crystal size. Thus, given $\varepsilon_r = 1$, H_{ic} increases and decreases with crystal size when $\eta > 1$ and $\eta < 1$, respectively.

A linear model is introduced to show how radiation broadens (or narrows) an ice crystal spectrum, where the time-scale for spectrum broadening relies on ε_r , η , crystal size, shape, air temperature and pressure. The time-scale is computed using observed parameters of ice crystals. It increases considerably with height through air temperature and pressure. Given $\eta = 0.5$, the time-scale is measured in minutes, hours and days at the 500, 250 and 100 hPa levels, respectively.

A nonlinear model that uses H_i as a prognostic variable is introduced to simulate the evolution of ice crystal spectrum due to radiation. Since H_{ic} varies with crystal size, water is redistributed between ice crystals with different sizes. When $\eta < 1$, smaller ice crystals shrink due to sublimation and larger ones grow due to vapour deposition, which results in precipitation formation even when ice water content is small and air is stationary.

The infrared ratio η approximately measures the relative magnitude of inward and outward infrared fluxes on the surface of an ice crystal. Owing to the great influence of clouds on η , the precipitation formation due to radiation is associated with clouds below. Based on the consistence between the characteristics of the radiative effect and the observations of subvisual clouds, it is inferred that the precipitation formation due to radiation exists in the upper troposphere.

However, the present parcel model needs to incorporate more physical processes so that its results are quantitatively comparable to field observations. Introducing ice crystal sedimentation, for example, is important in modelling ice crystal spectrum (e.g. Jensen *et al.*, 2007). A spectrally-resolved treatment of radiation (e.g. Stephens, 1983; Wu *et al.*, 2000) is important in the accurate determination of the infrared ratio η , the relative bulk absorption efficiency ε_r , and the absorbed solar flux F_s . With the full representation of the physics, the model can simulate optically-thin clouds so that its results are close to field observations.

Acknowledgements

This study is supported by the Office of Science, US Department of Energy through the Atmospheric Radiation Measurement (ARM) Program. The author appreciates Andy Heymsfield, Graeme Stephens, David O’C. Starr, Norihiko Fukuta and Ken Beard for clarifying many issues on cloud microphysics and radiation in the course of this study. He thanks Wei-Kuo Tao for kind support and Steve Lang for improving the manuscript. Special thanks are extended to two anonymous reviewers for their critical yet constructive comments.

Appendix A List of Symbols

a/b	: semi-major/semi-minor axis length
C	: stationary diffusion shape factor
C_p	: specific heat of dry air
D	: diffusivity of water vapour
e	: partial pressure of water vapour
e_c	: partial pressure of water vapour in the critical case, see (12)
E_{si}	: saturation vapour pressure over ice
f_m/f_Q	: ventilation factor for mass transfer/thermal diffusion
F_s	: solar flux absorbed by an ice crystal
F^+/F^-	: upward/downward infrared flux
F_α/F_β	: factor for the kinetic effect in heat/water vapour diffusion
g	: acceleration due to gravity
$H_i = e/E_{si}$: relative humidity with respect to ice
H_{ic}	: critical relative humidity, see (18)
K	: coefficient of thermal conductivity of dry air
L_s	: latent heat of sublimation
m	: mass of an ice crystal
$M(a)$: mass of ice crystals with semi-major axis length shorter than a
$N(a)$: number of ice crystals with semi-major axis length shorter than a
$r^* = S/4\pi C$: equivalent radius of an ice crystal, see (4)
R_d/R_v	: gas constant for dry air/water vapour
p	: air pressure
$p_0 = 10^5$ Pa	: reference pressure

$s = 4\pi r^{*2}$: area variable for modelling, see (28)
S	: surface area of an ice crystal
t	: time
T	: (air) temperature
T_e	: environmental temperature around an ice crystal
T_o	: absolute temperature of ice point
T_s	: surface temperature of an ice crystal
T_{sc}	: crystal surface temperature in the critical case, see (11)
α/β	: thermal accommodation/deposition coefficient
γ	: relative change of crystal surface temperature due to radiation in the critical case, see (13)
ϵ_0	: bulk absorption efficiency of an ice crystal for blackbody radiation
ϵ_r	: relative bulk absorption efficiency of an ice crystal for infrared radiation
η	: infrared ratio, see (9)
ρ_a/ρ_v	: density of air/water vapour
ρ_{si}	: saturation density of water vapour over ice
σ	: the Stefan–Boltzmann constant
τ	: time-scale for spectral broadening due to radiation, see (29)
χ	: ratio of the infrared flux to the conductive heat flux from air to an ice crystal while both air and the crystal are treated as blackbodies
Δt	: time step for numerical integration

References

- Auer Jr AH, Veal DL. 1970. The dimension of ice crystals in natural clouds. *J. Atmos. Sci.* **27**: 919–926.
- Beard KV, Pruppacher HR. 1971. A wind tunnel investigation of the rate of evaporation of small water drops falling at terminal velocity in air. *J. Atmos. Sci.* **28**: 1455–1464.
- Carstens JC. 1972. Comments on ‘Kinetics of hydrometeor growth from a vapor-spherical model’. *J. Atmos. Sci.* **29**: 588–591.
- Carstens JC, Podzimek J, Saad A. 1974. On the analysis of the condensational growth of a stationary cloud droplet in the vicinity of activation. *J. Atmos. Sci.* **31**: 592–596.
- Chapman S, Cowling TG. 1970. *The mathematical theory of non-uniform gases*. Cambridge University Press.
- Chou M-D, Ridgway WL, Yan MM-H. 1995. Parameterizations for water vapor IR radiative transfer in both the middle and lower atmospheres. *J. Atmos. Sci.* **52**: 1159–1167.
- Fu Q, Liou KN. 1992. On the correlated k -distribution method for radiative transfer in nonhomogeneous atmospheres. *J. Atmos. Sci.* **49**: 2139–2156.
- Fukuta N, Walter LA. 1970. Kinetics of hydrometeor growth from a vapor-spherical model. *J. Atmos. Sci.* **27**: 1160–1172.
- Hall WD, Pruppacher HR. 1976. The survival of ice particles falling from cirrus clouds in subsaturated air. *J. Atmos. Sci.* **33**: 1995–2006.
- Hallett J. 1987. Faceted snow crystals. *J. Opt. Soc. Am. A* **4**: 581–588.
- Hallett J, Arnott WP, Bailey MP, Hallett JT. 2002. ‘Ice crystals in cirrus.’ Pp. 41–77 in *Cirrus*, Lynch DK, Sassen K, Starr DO’C, Stephens G (eds). Oxford University Press: New York.
- Heymsfield AJ. 1972. Ice crystal terminal velocities. *J. Atmos. Sci.* **29**: 1348–1357.
- Heymsfield AJ. 1986. Ice particles observed in a cirriform cloud at -83°C and implications for polar stratospheric clouds. *J. Atmos. Sci.* **43**: 851–855.
- Heymsfield AJ, Iaquinta J. 2000. Cirrus crystal terminal velocities. *J. Atmos. Sci.* **57**: 916–938.
- Heymsfield AJ, Schmitt C, Bansemmer A. 2006. ‘Measurements in low latitude high altitude cirrus.’ *12th Conference on Cloud Physics*, 10–14 July 2006, Madison, Wisconsin, USA. American Meteorological Society.
- Houze Jr RA. 1977. Structure and dynamics of a tropical squall-line system. *Mon. Weather Rev.* **105**: 1540–1567.
- Houze Jr RA. 1982. Cloud clusters and large-scale vertical motion in the tropics. *J. Meteorol. Soc. Jpn* **60**: 396–410.
- Jensen EJ, Ackerman AS, Smith JA. 2007. Can overshooting convection dehydrate the tropical tropopause layer? *J. Geophys. Res.* **112**: D11209, doi: 10.29/2006JD007943.
- Ludlam FH. 1980. *Clouds and storms*. Pennsylvania State University Press.
- Lynch DK, Sassen K. 2002. ‘Subvisual cirrus.’ Pp. 256–264 in *Cirrus*, Lynch DK, Sassen K, Starr DO’C, Stephens G (eds). Oxford University Press: New York.
- Moncrieff MW. 2004. Analytic representation of the large-scale organization of tropical convection. *J. Atmos. Sci.* **61**: 1521–1538.
- Nesbitt SW, Zipser EJ, Cecil DJ. 2000. A census of precipitation features in the Tropics using TRMM: Radar, ice scattering, and lightning observations. *J. Climate* **13**: 4087–4106.
- Petch JC, Gray MEB. 2001. Sensitivity studies using a cloud-resolving model simulation of the tropical west Pacific. *Q. J. R. Meteorol. Soc.* **127**: 2287–2306.
- Pruppacher HR, Klett JD. 1997. *Microphysics of clouds and precipitation*. 2nd edition. Kluwer Academic.
- Raymond DJ, Zeng X. 2000. Instability and large-scale circulations in a two-column model of the tropical troposphere. *Q. J. R. Meteorol. Soc.* **126**: 3117–3135.
- Raymond DJ, Zeng X. 2005. Modelling tropical atmospheric convection in the context of the weak temperature gradient approximation. *Q. J. R. Meteorol. Soc.* **131**: 1301–1320.
- Riehl H, Malkus JS. 1958. On the heat balance in the equatorial trough zone. *Geophysica* **6**: 503–538.
- Roach WT. 1976. On the effect of radiative exchange on the growth by condensation of a cloud or fog droplet. *Q. J. R. Meteorol. Soc.* **102**: 361–372.
- Rogers RR, Yau MK. 1989. *A short course in cloud physics*. 3rd edition, Butterworth–Heinemann: Oxford.
- Shaw RA, Lamb D. 1999. Experimental determination of the thermal accommodation and condensation coefficients of water. *J. Chem. Phys.* **111**: 10659–10663.
- Simpson J, Adler RF, North GR. 1988. A proposed Tropical Rainfall Measuring Mission (TRMM) satellite. *Bull. Am. Meteorol. Soc.* **69**: 278–295.
- Starr DO’C, Quante M. 2002. ‘Dynamical processes in cirrus clouds: Concepts and models.’ Pp. 375–396 in *Cirrus*, Lynch DK, Sassen K, Starr DO’C, Stephens G (eds). Oxford University Press: New York.
- Stephens GL. 1983. The influence of radiative transfer on the mass and heat budgets of ice crystals falling in the atmosphere. *J. Atmos. Sci.* **40**: 1729–1739.
- Winker DM, Trepte CR. 1998. Laminar cirrus observed near the tropical tropopause by LITE. *Geophys. Res. Lett.* **25**: 3351–3354.
- Wu T, Cotton WR, Cheng WYY. 2000. Radiative effects on the diffusional growth of ice particles in cirrus clouds. *J. Atmos. Sci.* **57**: 2892–2904.
- Zeng X, Tao W-K, Zhang M, Peters-Lidard C, Lang S, Simpson J, Kumar S, Xie S, Eastman JL, Shie C-L, Geiger JV. 2007. Evaluating clouds in long-term cloud-resolving model simulations with observational data. *J. Atmos. Sci.* **64**: 4153–4177.
- Zipser EJ. 1969. The role of organized unsaturated convective downdrafts in the structure and rapid decay of an equatorial disturbance. *J. Appl. Meteorol.* **8**: 799–814.